Journal of Advanced Marine Engineering and Technology, Vol. 50, No. 2, pp. 110~117, 2026
J. Advanced Marine Engineering and Technology (JAMET)
https://doi.org/10.5916/jamet.2026.50.2.110

ISSN 2234-7925 (Print)
ISSN 2765-4796 (Online)
Original Paper

Development of a real-time integrated measurement system for polar ice load and navigation

Eun-Jin Oh[1] · Seong-Yeob Jeong[2] · Jung-Seok Ha†

(Received March 9, 2026 ; Revised March 30, 2026 ; Accepted April 7, 2026)

Abstract: Real-time synchronized measurement of hull strains, ship motions, ice conditions, and operating data is needed to interpret ship–ice interaction during full-scale polar navigation. This paper describes the onboard integrated measurement platform used on Araon and presents a pilot assessment of the exported data. The system combines 42 strain-gauge rosettes on the inner surface of the bow shell plating, a six-degree-of-freedom IMU, an electromagnetic ice-thickness sensor, six 4K IP cameras, and VDR/AMS interfaces on a common acquisition backbone. The representative dataset contained 14,857 synchronized samples at 50 Hz (297.1 s), 126 raw rosette channels, 42 engineering shear-strain channels, 42 principal-strain-angle channels, and six inertial-measurement channels. A continuity check of the 2024 Arctic archive covered 41 ice tests and about 24.1 h of synchronized context/response records, used only to confirm export continuity and quality flags. Event-level comparison showed that local strain bursts and global motion excursions can be examined on a common sample lattice, but the relation between windowed strain and peak accelerometer resultant remained weak ($R^2 = 0.21$). The platform is useful for synchronized monitoring and data archival, but routine load inversion still requires explicit UTC retention and finalized channel mapping.

Keywords: Polar navigation, Real-time ice-load monitoring, Integrated measurement system, Strain-gauge rosette, Inertial measurement unit

1. Introduction

Ships operating in ice-covered waters experience both localized hull response and whole-ship motions generated by ship-ice interaction. Reliable interpretation of these phenomena requires synchronized observation of structural strain, ship motion, operating condition, and surrounding ice environment. Full-scale studies have reported ice-load estimation from hull strain or from ship motion, but practical onboard systems that retain these heterogeneous signals on a common time base are still comparatively limited **[1][2]**.

For Araon, several prior studies have already addressed full-scale ice performance and ice-load interpretation. The early Arctic speed trial study summarized the relation among speed, ice thickness, ice strength, and propulsion power **[3]**. Subsequent work considered IMU-based global ice-load prediction **[4]**, local strain-based pressure or load estimation **[5]-[7]**, and a design-load-patch-based influence coefficient matrix for later ice-load estimation **[8]**, together with pack-ice resistance characteristics relevant to full-scale performance **[9]**. Those studies established the engineering value of the measurements themselves. They also showed that later interpretation depends strongly on the quality of synchronization, the stability of export formats, and the consistency of sensor naming between onboard records and analysis models.

The present paper therefore addresses the measurement-system side of the problem. Its scope is intentionally narrower than a campaign-wide load or performance study. The revision explicitly distinguishes measured structural response from reconstructed ice load. The strain-gauge and IMU records are treated here as synchronized response data that support later load

† Corresponding Author (ORCID: http://orcid.org/0000-0002-1976-6204): Senior Engineer, Ice Model Basin, Advanced-Intelligent Ship Research Division, Korea Research Institute of Ships & Ocean Engineering (KRISO), 32, 1312beon-gil, Yuseong-daero, Yuseong-gu, Daejeon, 34013, Korea, E-mail: jsha@kriso.re.kr, Tel: +82-42-866-3437

1 Senior Engineer, Ice Model Basin, Advanced-Intelligent Ship Research Division, Korea Research Institute of Ships and Ocean Engineering (KRISO), E-mail: ideal132@kriso.re.kr, Tel: 042-866-3434

2 Principal Researcher, Ice Model Basin, Advanced-Intelligent Ship Research Division, Korea Research Institute of Ships and Ocean Engineering (KRISO), E-mail: jsyeop@kriso.re.kr, Tel: 042-866-3432

reconstruction, not as direct load measurements.

The paper makes two specific contributions. First, it documents the current hardware-software architecture used to acquire, synchronize, visualize, and archive multi-sensor polar-navigation data on Araon. Second, it provides a conservative pilot assessment of the present export structure using one representative synchronized segment, while using the wider 2024 campaign only to check continuity and file-level data quality. Accordingly, the paper reports a measurement platform and its present limits rather than a finalized automatic load-inversion product.

2. Integrated Onboard Measurement Architecture

Accurate assessment of ship-ice interaction requires the simultaneous acquisition of local structural response, global ship motion, environmental context, and operating data. The platform was configured as an integrated onboard framework for collecting these heterogeneous data streams on a common processing backbone **[10]**.

The integrated onboard platform therefore comprises the following sensor modules and data pathways:

- Strain-gauge arrays mounted on the inner surface of the bow shell plating to capture structural strains that can support later local-load interpretation after sensor-to-model mapping is finalized;
- An inertial measurement unit (IMU) installed at the ship's centre of gravity to record 6-DOF motions for later comparison with local structural response and operating conditions;
- The ship's Voyage Data Recorder (VDR) interface to ingest thrust, shaft revolutions, speed over ground, trim and draft, providing the operational context for power–speed–resistance analysis;
- An electromagnetic induction sensor and a network of IP cameras located at the bow and shoulders to measure level-ice thickness and to document the surrounding ice conditions.

All sensor streams are integrated through a communication and storage backbone designed for onboard use and later shoreside analysis. The architecture is intentionally modular so that additional sensors or processing routines can be incorporated without changing the core acquisition framework.

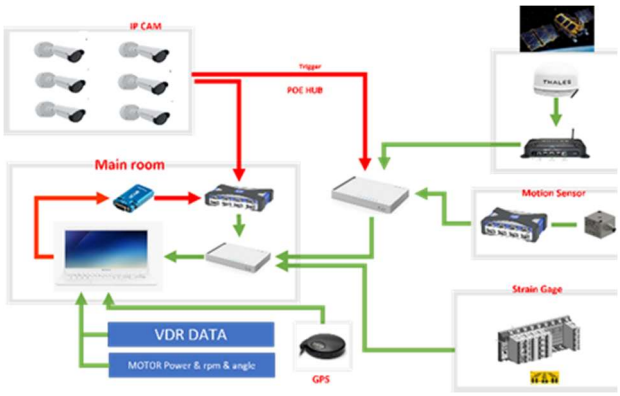

Figure 1: System architecture of the integrated onboard measurement platform

2.1 Hull-mounted Hardware Architecture

The onboard platform is configured to acquire in real time and on a common time base—four data domains that govern ship–ice interaction:

- ✓ Local structural response (hull strains)
- ✓ Global hull response (6-DOF motions)
- ✓ Ice-field environment (thickness, visual record)
- ✓ Operating parameters (power, speed, trim, etc.)

2.1.1 Local Ice-load Sensing

Forty-two three-axis resistive strain-gauge rosettes were bonded to the inner surface of the bow shell plating between frames 105 and 110. The term 'inner hull plating' is avoided here because it can be misunderstood as a reference to a separate inner-hull or double-bottom structure. External mounting on the wetted shell surface was not adopted because the gauges and lead wires would then be exposed directly to ice abrasion, coating damage, seawater ingress, and severe maintenance constraints during repeated polar operations. The installed rosettes therefore measure the structural response transmitted through the shell plate from the protected inner surface.

In the uploaded export, the rosettes appear as 126 raw A/B/C channels together with 42 SH and 42 AG derived outputs, all sampled at 50 Hz. Here, SH denotes the in-plane engineering shear strain derived from each 45-degree rosette, $SH = 2[\varepsilon_B - (\varepsilon_A + \varepsilon_C)/2]$, and AG denotes the corresponding principal-strain angle, $AG = 0.5\ \mathrm{atan2}(SH, \varepsilon_A - \varepsilon_C)$, reported in degrees and wrapped to 0-180 degrees. These channels measure

structural response; they are not interpreted in this paper as direct ice-pressure measurements.

2.1.2 Global Response Sensing

A 6-DOF inertial-measurement unit (IMU) is installed near the

Table 1: System architecture and data interfaces of the integrated onboard platform

Component	Model/Type	Installation point	Key specifications & role	Interface
Strain-gauge DAQ	HBM QuantumX-based DAQ	Edge DAQ rack (data-processing room)	Acquisition of rosette channels and derived outputs on the common 50 Hz backbone	Ethernet
DAQ software	HBM catman AP **[12]**	Same host PC	Real-time acquisition, visualization, logging, and export control	Software
Satellite link	Iridium Certus 700	External mast / shipboard link	Current ship-to-shore transfer and remote-access backbone; higher-bandwidth upgrades are planned	Ethernet
IP cameras x 6	4K network cameras	Bridge, bow shoulders (P&S), mid-side (P&S), stern	3840 x 2160 px at 30 fps, contextual video recording	PoE (power-over-Ethernet)
Laptop x 2	Dedicated acquisition and video nodes	Main data room	Separated numerical-acquisition node and video node	GbE (Gigabit Ethernet), USB
GNSS/PTP (Precision Time Protocol) source	GNSS receiver / timing source	Wheel-house roof	Reference timing source for onboard synchronization framework	NMEA / Ethernet
VDR/AMS interface	Shipboard recording interface	Bridge console	Collects power, rpm, speed, trim, draft, and related operating data	Gateway / LAN
Power-data hub	PoE switch and protected DC supply	Edge DAQ rack	Power and data distribution for cameras, DAQ, and network devices	PoE (power-over-Ethernet) / DC
Trigger / event logic	Software threshold logic	Edge DAQ host	Event tagging and synchronized export control	Software / Digital I/O

Table 2: Sensor channel configuration and current export status

Device type	Exported channels	Sampling rate	Current synchronization basis	Remarks
Strain-gauge rosettes	42 rosettes = 126 raw strain channels + 84 derived outputs (SH, AG)	50 Hz	Shared 50 Hz sample lattice and identical row count with IMU export	Port and starboard arrays between frames 105-110 (SH: engineering shear strain, με; AG: principal strain angle, deg)
IMU	6 numeric channels	50 Hz	Shared row count with strain export; TIME field blank in current CSV export	ACCEL_X/Y/Z and GYRO_X/Y/Z
EM ice-thickness transducer	1 channel (not included in uploaded CSV)	1 Hz	Integrated in platform design	Non-contact electromagnetic induction
4K network cameras	6 video streams	30 fps	Synchronized in platform design; frame-level UTC export should be retained	Contextual observation of ice-contact events
VDR/AMS / auxiliary	Operating variables (not included in uploaded CSV)	1 Hz or System rate	Integrated in platform design	Power, rpm, speed, trim, draft, etc.

ship center of gravity. Its six numerical channels are sampled on the same 50 Hz backbone used for the strain-gauge DAQ, which makes subsequent comparison between local structural response and global ship motion straightforward.

2.1.3 Ice-field Measurement

Level-ice thickness is measured in the 0–3 m range at 1 Hz by an electromagnetic induction (EM) transducer mounted 15° downward from bow-centreline. Because the EM method relies on the strong electrical-conductivity contrast between seawater and sea ice, it remains usable under fog, snowfall, and night-time conditions.

2.1.4 Visual Documentation

Six 4K IP cameras are installed at the bridge wings, bow stem, shoulders, and stern to document the ice-contact scene and surrounding environment during operation.

2.1.5 Operating Data Interface

Propulsive and navigation variables such as delivered power,

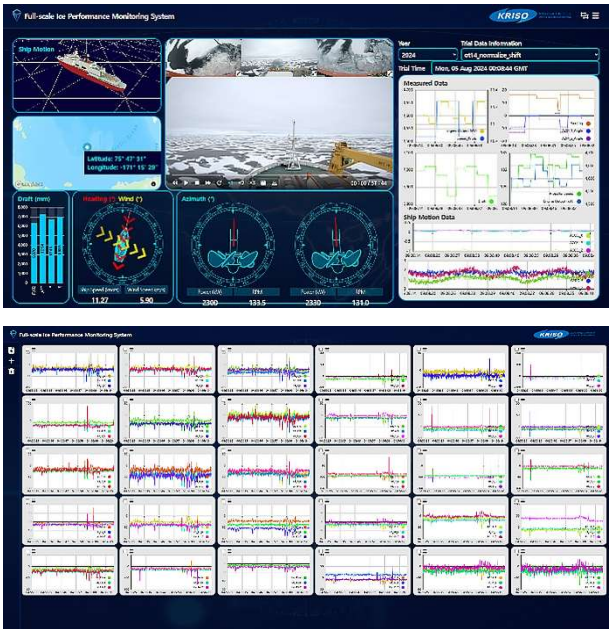

Figure 2: Example of the real-time onboard visualisation interface (top: integrated dashboard view for navigation and contextual video; bottom: multi-channel waveform quick-look view for strain-gauge monitoring)

shaft rpm, speed over ground, trim, and draft are interfaced from the shipboard recording systems to provide operational context for later analysis.

2.1.6 Time Synchronisation & Cabling

The platform is designed around a shared acquisition clock at the DAQ host and GNSS-referenced ship time, with time distribution compatible with Precision Time Protocol where applicable **[11]**. In the representative IMU CSV export, the dedicated TIME field was blank. The most plausible explanation is an export-template issue rather than loss of internal synchronization, because the IMU and strain-gauge files preserve identical row counts and the same 20 ms sample lattice over the representative segment. This inference is still weaker than direct timestamp auditability. For that reason, future exports should preserve explicit UTC timestamps for all numerical channels.

2.1.7 2024 System Upgrades

During the 2024 refit, several reliability-oriented updates were implemented, including extension of the EM calibration range, improvement of IMU continuity through firmware and buffering changes, upgrade of camera resolution, and additional short-circuit protection for strain-gauge wiring. No quantitative performance-gain values are claimed here.

2.2 Data acquisition and Current Export Structure

The platform employs a dedicated acquisition-and-synchronization module that collects strain-gauge, IMU, EM-thickness, camera, VDR/AMS, and GNSS streams on a shared onboard framework. **Table 2** summarizes the current sensor channels and export status used in this revision.

In the current implementation, waveform channels are sampled at 50 Hz and stored internally in 30 s NetCDF chunks together with metadata; external exports are generated as CSV for downstream analysis. This distinction between sampling interval and file-chunk duration is retained here because it affects later post-processing and auditability.

2.3 Onboard Data Processing and Visualization

When synchronized sensor streams arrive at the shipboard server they are processed in near-real time through signal decoding, unit conversion and filtering, generation of synchronized response indicators, and screen rendering. The current acquisition and display workflow is implemented through catman AP and associated export tools **[12]**.

Three-axis strain readings from each rosette are stored together with SH and AG derived outputs. A separate 21 x 21 influence-matrix workbook is available for one hull side and can support

Table 3: Cross-reference between DAQ channel labels and influence-matrix sensor IDs

DAQ label (port)	FE sensor ID (port)	DAQ label (starboard)	FE sensor ID (starboard)
LK_1	LK2	RK_1	RK2
LK_2	LK3	RK_2	RK3
LK_3	LK5	RK_3	RK5
LK_4	LK6	RK_4	RK6
LK_5	LK8	RK_5	RK8
LK_6	LK9	RK_6	RK9
LK_7	LK11	RK_7	RK11
LK_8	LK12	RK_8	RK12
LK_9	LK14	RK_9	RK14
LK_10	LK15	RK_10	RK15
LK_11	LK17	RK_11	RK17
LK_12	LK18	RK_12	RK18
LK_13	LK20	RK_13	RK20
LK_14	LK21	RK_14	RK21
LK_15	LK22	RK_15	RK22
LK_16	LK23	RK_16	RK23
LK_17	LK24	RK_17	RK24
LK_18	LK25	RK_18	RK25
LK_19	LK26	RK_19	RK26
LK_20	LK27	RK_20	RK27
LK_21	LK28	RK_21	RK28

later matrix-based load reconstruction; a recent design-load-patch-based derivation of such a matrix for Araon was reported separately **[8]**. To reduce naming ambiguity at the interface between the onboard export and the analysis model, **Table 3** lists the one-to-one correspondence adopted in the present study between the sequential DAQ channel labels and the sensor IDs defined in the influence-matrix workbook for one hull side.

The two naming systems are not numerically identical, so **Table 3** is used as a cross-reference for later matrix-based interpretation. The present paper does not further discuss the origin of the non-contiguous workbook numbering. The starboard side follows the corresponding RK series. This clarification is sufficient for traceable channel-to-sensor correspondence in the present paper, but full pressure back-calculation is still not reported because a fully audited inversion chain, including sign convention and downstream force integration, has not yet been frozen.

2.4 Remote Transfer and Archival Platform

Because raw ice-trial data can reach tens of gigabytes per day, the platform adopts a staged workflow consisting of onboard storage, selective ship-to-shore transfer, and shore-side archival. In the 2024 configuration examined here, higher-bandwidth satellite transfer was not yet treated as a demonstrated capability of the uploaded dataset.

2.5 Environmental Hardening and System Control

The platform is intended for use in cold, humid, and saline polar environments, so the hardware design emphasizes power redundancy, local heating, waterproof encapsulation, and robust cabling.

The measuring network is supplied from the ship AC switchboard through a protected DC conversion stage, and critical instruments can be buffered by UPS (uninterruptible power supply) hardware to reduce data corruption during short disturbances.

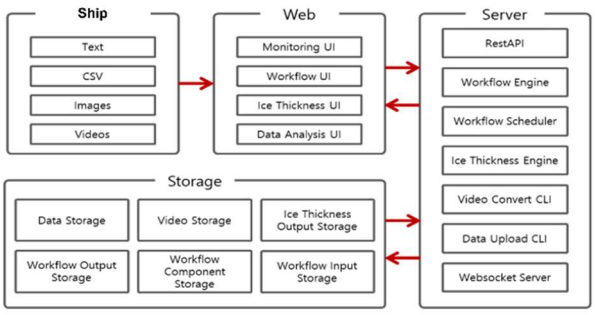

Figure 3: Remote-transfer and shore-side archiving workflow

Outdoor instruments are housed in insulated enclosures with local heating control to mitigate icing and condensation.

External links use cold-resistant Ethernet and sealed penetrations to withstand seawater spray and repeated deck operations.

Further optimization of the thermal-management strategy remains possible, but this topic is outside the scope of the present paper.

3. Representative Arctic Dataset and Pilot Assessment

3.1 Campaign Context and Representativeness

The representative synchronized segment used for detailed plots in this paper contains 14,857 samples at 50 Hz, corresponding to approximately 297.1 s. To clarify how representative that segment is with respect to the 2024 campaign, the revised assessment also checked continuity across the processed campaign archive. The broader archive contained 41 official ice tests (OT02-OT42), 4,335,303 synchronized context/response rows, and approximately 24.08 h of records after file concatenation. That broader corpus was used only to confirm that synchronized exports existed across the campaign and to identify file-level quality flags; it was not used here to claim campaign-wide performance or load statistics.

3.2 Representative Synchronized Response and Event Level Interpretation

The representative strain-gauge export contains 126 raw A/B/C strain channels, 42 SH channels, and 42 AG channels. The synchronized IMU export contains six numerical channels. No missing numerical samples were found in the representative strain-gauge channels or in the six IMU measurement channels.

For event screening, the revision uses the sample-wise maximum absolute shear-strain response, $S_{H,max} = \max_j |SH_j|$, and the accelerometer resultant deviation $|a_{res} - \mathrm{median}(a_{res})|$,

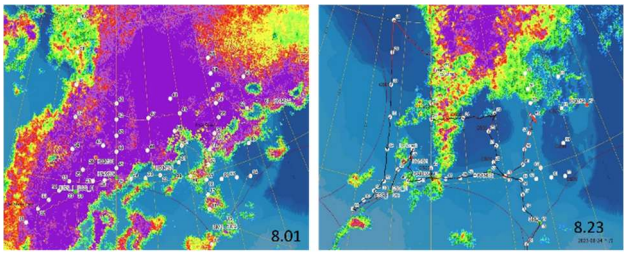

Figure 4: Representative operating area and contextual ice-condition information used during the August 2024 Arctic Voyage

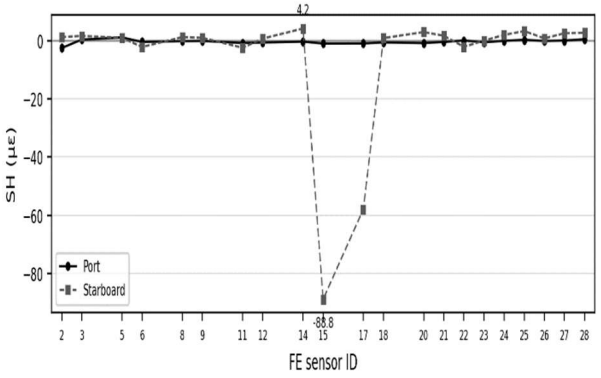

Figure 5: Event-time SH values arranged by FE sensor ID for subsequent influence-matrix mapping

where a_res = sqrt(a_x² + a_y² + a_z²). Within the zoomed interval of **Figure 6(b)** (81.0-85.1 s), S_H,max reached 88.8 microstrain at 83.14 s, whereas the peak accelerometer resultant deviation of 0.047 g occurred at 82.00 s. The two peaks fall within the same short event window but are not coincident. This offset indicates that localized structural bursts and whole-ship motion excursions are related, yet they cannot be treated as a single synchronized scalar peak.

Figure 5 reorganizes the sample-wise SH values at the event time of 83.14 s according to the FE sensor IDs used in the influence matrix. At that instant, the signed SH values ranged from approximately -88.8 to +4.2 με across the 42 channels. The strongest negative response occurred on the starboard side at FE sensor ID 15 (DAQ channel RK_10), and the next strongest negative response appeared at FE sensor ID 17 (DAQ channel RK_11). Most port-side channels remained within only a few microstrain of zero. This channel-wise pattern is consistent with a localized and spatially non-uniform structural response field. It does not, by itself, determine contact pressure magnitude, exact contact location, or pressure-patch geometry, because those quantities require a fully audited inversion step.

Figure 6 presents a verified example of synchronized local and global response indicators extracted directly from the uploaded files. **Figure 6(a)** shows the full-record response, where the left axis represents the maximum absolute SH strain across the available SH channels and the right axis represents the accelerometer resultant deviation derived from the IMU export. **Figure 6(b)** enlarges the 81.0–85.1 s interval and shows that local strain bursts and the global motion indicator can be compared on the same 50 Hz sample grid within a single synchronized segment. In Figure 6, the accelerometer resultant is a_res = √ (a_x²

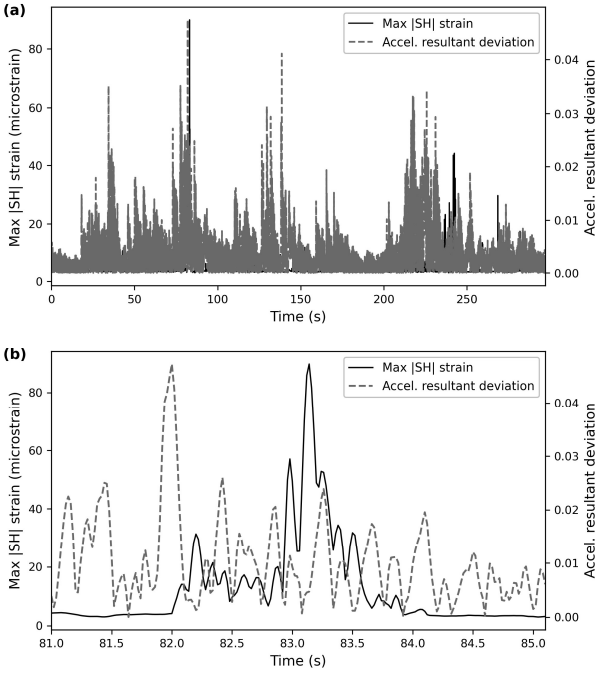

Figure 6: Verified synchronized local-strain and global-motion indicators extracted from the uploaded segment: (a) full-record time history of the maximum absolute SH strain and the accelerometer resultant deviation; (b) zoomed view of the 81.0–85.1 s interval

+ a_y² + a_z²) (as exported by the IMU, in g-units), and the plotted deviation is |a_res − median(a_res)|. The left axis quantity is max_j |SH_j|, i.e., the maximum absolute shear strain across the 42 SH channels at each sample.

The exploratory relation in **Figure 7** yields $R^2 = 0.21$ between the non-overlapping 2 s mean absolute raw strain and the 2 s peak accelerometer resultant. This weak relation is reported explicitly because it argues against reducing localized hull response and whole-ship motion to a single scalar conversion in the present dataset. The low coefficient of determination indicates that these two screening metrics do not, by themselves, capture the underlying physical relation strongly enough for predictive use. Accordingly, no regression-based load surrogate is proposed here. The figure should therefore be read only as a screening plot showing that the two indicators may rise within the same short event window, while their amplitudes and peak timings are not governed by a simple one-to-one relation. Physically, this is reasonable: the local strain metric depends on contact position and the local structural load path, whereas the accelerometer resultant reflects the rigid-body motion response of the whole ship.

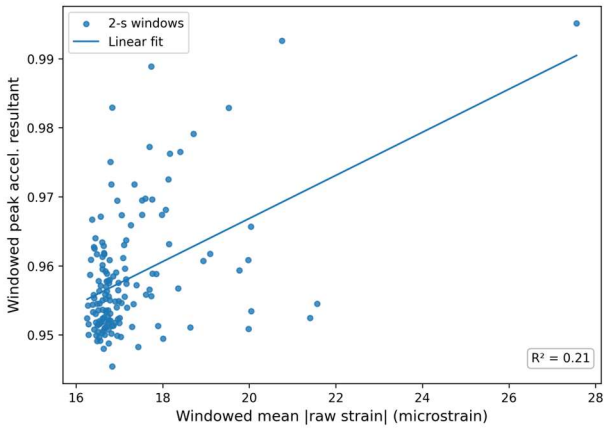

Figure 7: Exploratory relationship between the 2-s-window mean absolute raw strain and the 2-s-window peak accelerometer resultant in the uploaded segment ($R^2 = 0.21$)

Table 4: Representative Segment and Wider Campaign Context

Item	Verified status / value
Representative synchronized segment	14,857 samples at 50 Hz (approximately 297.1 s)
Representative strain export	126 raw A/B/C channels + 42 SH + 42 AG
Representative IMU export	6 numeric channels; TIME field blank in current CSV template
Missing numerical samples in representative SG / IMU channels	None observed
Processed 2024 campaign continuity check	41 official ice tests (OT02-OT42)
Total synchronized context / response rows in processed campaign archive	4,335,303
Total record length in processed campaign archive	24.08 h

Table 4 therefore summarises the representative uploaded files and the current processing status, rather than presenting full-voyage structural-design comparisons.

3.3 Practical Implications for Routine Operation

The revised assessment confirms that the current platform can stably export high-dimensional strain-gauge and IMU data on a common sample lattice. At the same time, three implementation-level items remain necessary before routine real-time load inversion should be reported as an operational product: (i) explicit UTC timestamp retention in every export, (ii) finalized DAQ-to-FE sensor mapping with audited sign and side conventions, and (iii) fixed event-tagging rules for selecting comparable impact events.

These remaining tasks do not undermine the value of the present platform. They define the boundary of what can be claimed from the current files. The platform can already be regarded as a practical integrated measurement and data-management system for full-scale monitoring, event screening, and later ship-ice interaction analysis. It should not yet be described as a finalized automatic pressure-inversion product.

4. Conclusion

This paper presented the current configuration of the integrated onboard platform used on Araon to acquire, synchronize, visualize, and archive polar-operation data. The revision also clarified several points raised during review: the strain gauges are mounted on the inner surface of the bow shell plating for practical survivability and maintainability; the DAQ-to-FE sensor correspondence used by the influence-matrix workbook is now documented explicitly; the blank IMU TIME field is treated as an export-level deficiency rather than as direct evidence of synchronization loss; and the representative segment is now placed in the context of a wider 2024 campaign archive.

The representative files confirm synchronized export of 210 strain-related columns and six IMU channels on a common 50 Hz sample lattice over approximately 297.1 s. The wider 2024 archive shows that such synchronized context/response exports were available across 41 official ice tests. Event-level comparison demonstrates that local strain bursts and global motion excursions can be examined on the same sample grid, while the weak scalar strain-motion relation ($R^2 = 0.21$) indicates that simple one-parameter surrogates are insufficient for load inference. Accordingly, the present platform is best regarded as a practical integrated measurement backbone for full-scale monitoring and traceable data archival. Routine quantitative load inversion still requires explicit UTC retention in the export files and a fully audited inversion workflow built on the documented channel-to-sensor mapping.

Acknowledgement

This research was supported by the Korea Research Institute of Ships and Ocean Engineering (KRISO) through a grant from the endowment project titled “Development of International-Level Performance Evaluation Technology for Arctic Navigation Vessels,” funded by a government-funded research program (PET0040).

Author Contributions

Author Contributions: Conceptualization, J. -S. Ha; Methodology, J. -S. Ha; Software, E. -J. Oh; Validation, Jung-Seok Ha; Formal Analysis, J. -S. Ha; Investigation, J. -S. Ha; Resources, J. -S. Ha; Data Curation, J. -S. Ha; Writing—Original Draft Preparation, J. -S. Ha; Writing—Review & Editing, J. -S. Ha; Visualization, J. -S. Ha; Supervision, J. -S. Ha; Project Administration, S. -Y. Jeong; Funding Acquisition, S. -Y. Jeong.

References

[1] B. Leira, L. Borsheim, O. Espeland, and J. Amdahl, “Ice-load estimation for a ship hull based on continuous response monitoring,” Proceedings of the Institution of Mechanical Engineers, Part M: Journal of Engineering for the Maritime Environment, vol. 223, no. 4, pp. 529-540, 2009. https://doi.org/10.1243/14750902JEME141

[2] H. Nyseth, R. Frederking, and B. Sand, “Evaluation of global ice load impacts based on real-time monitoring of ship motions,” Proceedings of the 22nd International Conference on Port and Ocean Engineering under Arctic Conditions (POAC'13), Espoo, Finland, June 9-13, Paper No. 135, 2013.

[3] H. S. Kim, C. J. Lee, S. Y. Jeong, and K. S. Choi, “A study on the speed sea trial on the ice field for ice breaking research vessel "Araon," Journal of the Society of Naval Architects of Korea, vol. 48, no. 5, pp. 421-425, 2011.

[4] S. C. Lee, S. Park, K. Choi, and S. Y. Jeong, “Prediction of ice loads on Korean IBRV ARAON with 6-DOF inertial measurement system during trials of Chukchi and East Siberian Seas,” Ocean Engineering, vol. 151, pp. 23-32, 2018. https://doi.org/10.1016/j.oceaneng.2018.01.010

[5] T. K. Lee, T. W. Kim, C. W. Rim, and S. Kim, “A study on calculation of local ice pressures for ARAON based on data measured at arctic sea,” Journal of Ocean Engineering and Technology, vol. 27, no. 5, pp. 88-92, 2013.

[6] J. K. Min, K. Choi, E. J. Cheon, and J. M. Kim, “Ice load estimation procedures for IBRV ARAON by analyzing shear strain data measured in arctic sea,” Journal of Ocean Engineering and Technology, vol. 30, no. 6, pp. 468-473, 2016.

[7] M. Jeon, K. Choi, J. K. Min, and J. S. Ha, “Estimation of local ice load by analyzing shear strain data from the IBRV ARAON's 2016 Arctic voyage,” International Journal of Naval Architecture and Ocean Engineering, vol. 10, no. 3, pp. 421-425, 2018.

[8] J. S. Ha, E. J. Oh, D. H. Kim, and B. R. Ryu, “New influence coefficient matrix based on design load patch for estimating ice loads on icebreaker research vessel,” Journal of the Korean Society of Marine Environment & Safety, vol. 31, no. 3, pp. 383-389, 2025. https://doi.org/10.7837/kosomes.2025.31.3.383

[9] S. Y. Jeong, K. Choi, and H. S. Kim, “Investigation of ship resistance characteristics under pack ice conditions,” Ocean Engineering, vol. 219, p. 108264, 2021. https://doi.org/10.1016/j.oceaneng.2020.108264

[10] S. Y. Jeong and E. J. Oh, “A simplified method to predict full-scale ship performance in pack ice fields,” Journal of Advanced Marine Engineering and Technology, vol. 49, no. 6, pp. 510-517, 2025.

[11] IEEE, 2019. IEEE Standard for a Precision Clock Synchronization Protocol for Networked Measurement and Control Systems (IEEE Std 1588-2019). IEEE Standards Association.

[12] Hottinger Bruel & Kjaer (HBK), 2022. catman AP 2022 User Manual. HBK Technical Documentation.